·技术方法·

腰椎 L_4～L_5活动节段有限元模型的建立与验证

刘耀升[1*]，陈其昕[1]，廖胜辉[2]，唐小君[1]，李方财[1]，吴浩波[1]，余世策[3]
(1.浙江大学医学院附属第二医院骨科，杭州 310009；2.浙江大学计算机学院 CAD&CG 国家重点实验室，杭州 310027；3. 浙江大学建筑工程学院结构工程研究所，杭州 310027)

[摘要] **目的**：采用一种新型计算机辅助设计(CAD)方法精确建立腰椎 L_4～L_5节段三维非线性有限元模型并进行充分验证。**方法**：采用改良的"非种子区域分割方法"提取腰椎 CT 图像数据中目标区域得到二值图像，用 Marching Cubes 方法由二值数据生成初始表面模型。采用反映腰椎生理曲度的"最佳切割平面"从初始表面模型获得非平行的切割轮廓线并建立"分段线性子空间"，后者经仿射变换到"规则子空间"快速重构腰椎曲面，最后逆变换恢复腰椎原三维空间形状特征。将表面模型所有结点的坐标数据和三角面片信息导入 ANSYS 进行网格划分精确建立 L_4～L_5节段三维非线性有限元模型，并进行加载验证。**结果**：所构建的 L_4～L_5活动节段有限元模型包括 94 794 个 Solid 单元，1 196 个 Link 单元，1 170 个 Shell 单元，768 个 Target 单元，464 个 Contact 单元；同时包含了几何非线性、材料非线性与接触非线性 3 种非线性类型。不同载荷条件下 L_4～L_5节段有限元模型的移位/旋转角度、椎间盘内压等预测结果与文献中相同载荷条件的试验生物力学结果相符合。**结论**：基于先进算法建立的腰椎 L_4～L_5节段表面模型实现了二值图像提取、腰椎曲面重构的全数字化过程，具有极佳的仿真效果。

[关键词] 生物力学；有限元方法；计算机辅助设计；腰椎；表面模型；验证
[中图分类号] R 318.08 **[文献标识码]** A **[文章编号]** 0258-879X(2006)06-0665-05

Development and validation of a finite element model for lumbar motion segment (L_4-L_5)

LIU Yao-sheng[1*], CHEN Qi-xin[1], LIAO Sheng-hui[2], TANG Xiao-jun[1], LI Fang-cai[1], WU Hao-bo[1], YU Shi-ce[3] (1. Department of Orthopedics Surgery, the Second Affiliated Hospital, Zhejiang University, Hangzhou 310009, China; 2. State Key Laboratory of CAD and CG, Department of Computer Science and Engineering, Zhejiang University, Hangzhou 310027; 3. Structural Engineering Institute, College of Architecture Engineering, Zhejiang University, Hangzhou 310027)

[ABSTRACT] **Objective**: To develop and validate an accurate three-dimensional geometrical and mechanical finite element(FE) model of the lumbar L_4-L_5 segment using a new computer-aided designing (CAD) method. **Methods**: First, a modified "non-seed region segmentation" was done to extract the interest region in the CT image and to obtain a binary image, from which the iso-surface of vertebral body was produced by a discretized marching cubes algorithm. Second, "best cross-section planes" representing the morphologic characteristics of physiological lordosis were used for the initial iso-surface model, forming a "non-regular piecewise subspace". This subspace and the embedded iso-surface model were subsequently transformed by local affine transforms to a "regular subspace", in which a surface mesh of high quality was generated quickly. Finally, a reverse transform procedure was employed to restore the original three-dimensional (3D) image of the lumbar surface mesh of lumbar L_4-L_5. All coordinate dada of nodal points and message of triangular patches of the surface model were then subjected to ANSYS for the three-dimensional FE mesh construction. An accurate 3D non-linear FE model of lumbar motion segment (L_4-L_5) was developed and validated against published data. **Results**: The constructed FE model of lumbar L_4-L_5 consisted of 94 794 solid elements, 1 196 link elements, 1 170 shell elements, 768 target elements and 464 contact elements, and included geometrical, material and contact non-linearities. The predicted results of lumbar L_4-L_5 segment were closely correlated with published results of experimental biomechanics in terms of axial displacement, segment rotation and intradiscal pressure under similar load condition. **Conclusion**: Based on advanced algorithm, this constructed surface model of L_4-L_5 segment is capable to perform whole digitalized binary image extraction and reconstruction of the lumbar surface with excellent simulation results.

[KEY WORDS] biomechanics; finite element method; computer aided design; lumbar spine; surface model; validation
[Acad J Sec Mil Med Univ, 2006, 27(6): 665-669]

有限元(finite element, FE)方法是体外试验生物力学研究方法的必要补充和有效"替代工具"，它不仅能较好地模拟复杂的力学环境，而且可以提供其他实验生物力学方法不能直接测量的结构内部力学反应，从而获得全域性信息。脊柱 FE 模型预测结果的有效性取决于它对脊柱复杂解剖结构模

[基金项目] 卫生部科学研究基金重点项目(WKJ 2005-Z-046). Supported by the Key Program of Science Research of the Ministry of Health(WKJ 2005-Z-046).

[作者简介] 刘耀升，博士，主治医师.
* Corresponding author. E-mail: liuyaosheng001@yahoo.com.cn

拟的准确性，因此构建具有精确表面形态的腰椎活动节段几何模型是腰椎 FE 建模过程的关键。目前，腰椎 FE 建模方法多首先在其他计算机辅助设计（computer aided design，CAD）软件中创建几何模型，然后通过数据接口导入 FE 软件进行网格划分。这种间接建模法虽然建模效率、网格划分质量较 Goel 等[1]的直接建模法有所提高，但在从 CT 扫描图像获取建模数据时，多数建模方法仍局限于将每个单层图像的轮廓形状信息叠加在一起获取椎体的原始几何信息；同时，生成有限元模型中的单元是以平齐于 CT 扫描平面的方式排列，未能精确反映脊柱复杂解剖结构特征[2]。本研究采用一种新型 CAD 方法，精确建立腰椎 L_4～L_5 活动节段三维非线性有限元模型，同时对模型加载运算结果进行充分验证。

1　方法和结果

1.1　*腰椎实体表面模型的建立及三维坐标的获取*　选取一名 32 岁健康中国男性志愿者为建模素材，采用 SOMATOM SENSATION 16 螺旋 CT 机对其腰椎 L_4～L_5 节段进行连续的平行扫描，扫描层厚 0.75 mm；图像数据刻录存盘后，导入医学图像可视化研究平台。由于正常腰椎左右两边可视为对称性结构，仅取腰椎 L_4～L_5 节段右半边 1/2 进行实体建模。

1.1.1　*二值图像的提取*　采用“非种子区域分割方法”提取 L_4～L_5 节段的二值图像。主要步骤如下：(1)对 CT 图像进行中值滤波预处理。(2)去除图像中噪声影响，调整图像的灰度值分布，加强图像的对比度。(3)用一种改进的种子填充算法分割出连通的背景区域和软组织区域。对每幅图像，从一个非腰椎点出发，一般选择点(0,0)，迭代加入满足阈值条件的与其连通的非边界点，直到把连通的软组织和背景区域分离出来，剩下的各个连通的独立区域则是腰椎节段骨质所在的区域(还有可能的噪声区域)，从而得到各个层面的二值图像，并对这些二值图像进行优化分割。(4)将各层的二值图像叠加成体数据，利用腰椎区域的空间连通性进行三维的区域增长，并对其他区域进行反值填充，自动去掉噪声和其他不必要的骨质区域的影响，得到最终的二值图像。

1.1.2　*表面模型的建立*　采用一系列有针对性的方法由最终的二值图像建立 L_4～L_5 节段表面模型。主要流程如下：(1)用 Marching Cubes 方法由 CT 图像数据生成 L_4～L_5 节段表面模型。(2)用相同大小的 4 个切割平面放置于 L_4、L_5 椎体的近似上下平面处，插值决定中间切割平面的位置(图 1A)。这些切割平面能抽取椎体最佳几何信息，被称为“最佳切割平面”。(3)连接这些“最佳切割平面”组成一个“分段线性子空间”，用仿射变换将该子空间和其中嵌入的非平行的切割轮廓信息变换到一个规则的子空间，使各层之间切割轮廓相互平行并有相同的层间距。(4)将规则的子空间划分成一个规则的背景结构网格，并把切割轮廓映射到规则的结构网格点上并以此生成整数距离场。(5)从整数距离场快速抽取生成新的规则的表面模型，先将新表面模型恢复到平面切割轮廓的所在位置，再用逆仿射变换恢复其原始三维空间中的位置，最后生成腰椎 L_4～L_5 活动节段右半边三维表面模型(图 1B)。模型共包括 6 537 个结点，14 686 个三角面片。

1.2　*有限元模型的建立*　将 L_4～L_5 节段表面模型的结点坐标及三角面片信息导入 ANSYS（Inc. Pennsylvania，USA）有限元软件，采用自底向上的方法建立 L_4～L_5 节段右半面几何模型。利用有限元软件的自由网格划分功能进行网格划分，通过映射方式对称地创建另一半有限元模型，得到 L_4～L_5 活动节段完整有限元模型(图 1C)。复杂腰椎 L_4～L_5 活动节段完整有限元模型包括共 94 794 个实体单元，1 196个缆单元，1 170 个壳单元，768 个目标单元，464 个接触单元，总计共 134 518 个结点。模型包含了几何非线性、材料非线性、接触非线性 3 种结构非线性类型。各部位的单元类型、单元数和材料属性见表 1[1,3]。

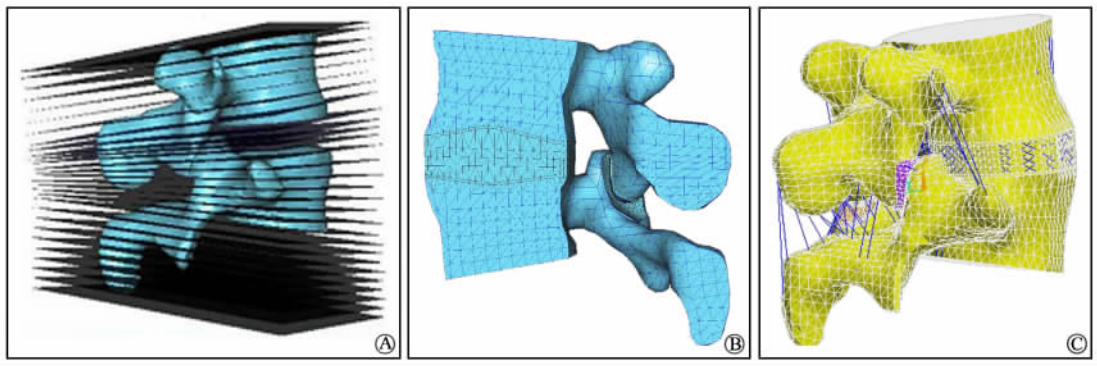

图 1　L_4～L_5 活动节段三维非线性有限元模型的建立

Fig 1　3D non-linear finite element model of lumbar L_4-L_5 motion segment

A：Marching cubes surface and non-parallel best cross-sectional planes；B：One-side surface model of lumbar L_4-L_5 motion segment；C：An intact 3D non-linear finite element model of lumbar L_4-L_5 motion segment

表 1 完整 L_4～L_5有限元模型单元类型、单元数、材料特性表

Tab 1 Element types, element numbers and material properties used in intact FE model of L_4-L_5

Material	Type of Element	No. of Elements	Elastic Modulus (MPa)/ Poisson's ratio	Area(A/mm^2)
Cortical bone	6-node solid	1 700	12 000/0.3	-
Cancellous bone	10 node-solid	29 912	100/0.2	-
End-plate	10 node-solid	14 500	500/0.25	-
Posterior element	10 node-solid	21 332	35 000/0.25	-
Annulus matrix	10 node-solid	10 287	4.2/0.45	-
Nucleus	10 node-solid	14 672	1.0/0.499	-
Annulus fiber	2 node-Link	1 146	Nonlinear	-
Articular cartilage	10 node-solid	1 172	10 000/0.3	-
Facet contact	Sliding surfacecontact element	1 172	-	-
Anterior longitudinal	2 node-Link	9	7.8 (ε< 12.0%), 20.0 (ε>12.0%)	75.9
Posterior longitudinal	2 node-Link	5	10.0 (ε< 11.0%), 20.0 (ε>11.0%)	51.8
Ligamentum flamvum	2 node-Link	6	15.0 (ε<6.2%), 19.5 (ε>6.2%)	78.7
Intertransverse	2 node-Link	6	10.0 (ε<18.0%), 58.7 (ε>18.0%)	2.0
Capsular	2 node-Link	10	7.5 (ε<25.0%), 32.9 (ε>25.0%)	102.5
Interspinous	2 node-Link	10	10.0 (ε<14.0%), 11.6 (ε>14.0%)	36.3
Superspinous	2 node-Link	4	8.0 (ε<20.0%), 15.0 (ε>20.0%)	75.7

1.2.1 *椎体和后部结构* 椎体皮质骨用 6 结点三角面薄壳单元模拟,单元厚度设定为 1.0 mm。椎体松质骨、终板、椎间盘纤维环基质以及后部结构,包括椎弓根、峡部、终板、棘突、横突、小关节突以及关节软骨由 10 结点四面体等参元进行结构离散。

1.2.2 *椎间盘* 椎间盘髓核被模拟为不可压缩的黏弹性液体,其体积模量为 1 666.70 MPa。髓核的体积占椎间盘体积的 48.87%。椎间盘纤维环由基质与埋在基质中的胶原纤维所构成的混合体表示,前者由 3 层连续性环状体构成。纤维环纤维由 8 层只承受张应力的索单元构建,纤维在环状体中呈剪刀状方式走行,并与椎间盘平面成平均±30°的夹角[4]。纤维体积占纤维环总体积的 19%,各层纤维的横截面积自外向内逐渐减小,纤维环纤维的弹塑性应力应变关系曲线参考文献[5]。椎间盘的上下表面由 1.0 mm 厚的软骨终板构成,L_4下终板与 L_5上终板凹陷角分别设为 156.9°和 165.6°。

1.2.3 *关节软骨* 关节突软骨层厚 0.5 mm,关节软骨层的表面接触选用面-面接触单元模拟(无摩擦的滑动表面接触单元)。接触单元的初始间距为 0.6 mm,摩擦系数为 0。关节软骨的材料属性被处理为线弹性,其弹性模量设定 10 000 MPa[3]。

1.2.4 *韧带* 有限元模型包含的前纵、后纵、棘上、棘间、横突间韧带以及黄韧带和关节囊韧带均采用超弹性索单元模拟,单元的位置、横截面积及长度决定于各组韧带的实际解剖结构。

1.3 *边界与负载条件* 约束 L_5椎体和棘突底面上所有结点平移和转动共 6 个自由度,垂直压缩载荷 3 000 N,分 10 步逐步施加于 L_4椎体顶面。屈曲、后伸力矩载荷,侧屈、扭曲力矩载荷 15 N,分别以结点载荷的形式分 10 步施加于 L_4椎体顶面前后端结点和左右侧端结点上,力矩载荷施加前均无预载。

1.4 *模型验证* 不同载荷条件下 L_4～L_5节段有限元模型的预测结果与相同边界条件下的体外实验生物力学研究结果[6~14]近似。轴向压缩载荷条件下,L_4～L_5有限元模型的压缩-位移曲线位于 Brown[6]、Markolf[7]、Virgin[9]等的实验研究曲线之间(图 2A),压缩载荷增加,L_4～L_5节段椎间盘刚度亦轻度增加;压缩-椎间盘内压力曲线位于 Nachemson[10]与 Rolander[11]的实验研究曲线之间(图 2B)。

屈曲、伸直载荷条件下,L_4～L_5有限元模型的扭矩载荷-旋转角度曲线的非线性走行趋势与 White[13]、Schultz[14]等的实验研究结果相一致(图 2C、2D),有限元模型的屈曲-旋转角度曲线低于相应的实验生物力学研究曲线。

侧屈、扭转载荷条件下,L_4～L_5有限元模型的载荷-旋转角度曲线呈线性走行(图 2E、2F),有限元模型的预测结果与 Markolf[7]、Tencer[12]等的实验研究结果近似。与实验生物力学研究结果相比,侧屈载荷条件下,有限元模型的刚度较大。

2 讨 论

本研究采用非平行的"最佳切割平面"获取椎体的几何信息,并将其映射到规则的背景结构体网格中生成表面模型,最后恢复椎体的原始几何形状,所构建的腰椎三维表面模型具有以下特点:(1)根据腰椎 CT 断层图像的灰度分布特征以及腰椎的形状特点,分别提出"非种子区域分割方法"、"最佳切割平面"、"分段线性子空间"和"规则子空间"等抽取腰椎 CT 数据的二值图像、最佳切割轮廓线和基于这些断层轮廓线重构腰椎曲面的特定算法,采用这些算法构建腰椎活

动节段表面模型便捷、迅速，且具有极佳的仿真效果。(2)生成的单元形状规则，大小、疏密过渡光滑，且排列方向与椎体的朝向非常符合，保证了有限元模型网格划分的质量。(3)CAD 医学平台提供了腰椎表面模型所有结点的三维坐标数据和三角面片结点的编码数据，数据文本文件导入 ANSYS 有限元软件后，可直接由点到面，由面到体重建腰椎几何模型，避免了实体模型导入有限元软件时数据接口无法衔接，简化了腰椎几何模型的建模过程。(4)由三角面片生成的四面体单元最适用于具有复杂边界曲面的不规则椎体结构的离散。(5)单元网格划分运用自适应的模式，对椎间盘、终板、关节突关节等应力集中部位进行网格加密，如 L_4 下关节突与 L_5 上关节突关节面分别采用 708 个和 464 个单元进行结构离散，远远多于目前文献中腰椎 FE 模型相应部位的单元数，减少了 FE 模型的几何离散误差。(6)腰椎三维 FE 模型的计算属于高度非线性问题，FE 计算中选用的条件共轭梯度法求解器与一般求解器相比对病态矩阵更具有稳固性，特别适合于高度非线性大型结构的求解，极大地提高了计算速度。

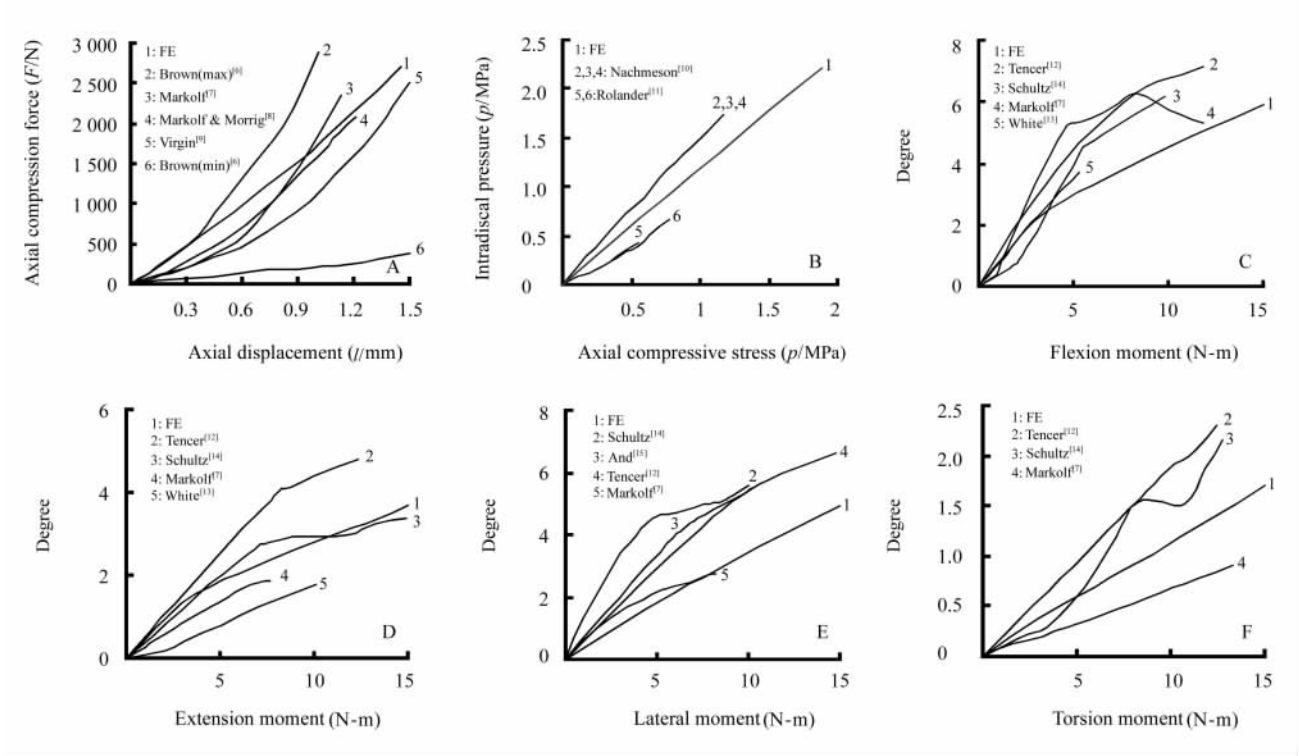

图 2　有限元模型与实验生物力学研究的比较

Fig 2　Comparison between FE results and the results of experimental studies

A: Axial compressive force *versus* axial displacement. FE results *versus* results of experimental studies, *in vitro* testing; B: Intradisc pressure *versus* axial compressive stress. FE results *versus* results of experimental studies, *in vitro* testing; C: Segment flexion under pure sagittal moment for FE model. FE results *versus* results of experimental studies, *in vitro* testing; D: Segment extension under pure sagittal moment for FE model. FE results *versus* results from experimental studies, *in vitro* testing; E: Segment lateral bending under pure frontal moment for FE model. FE results *versus* results of experimental studies, *in vitro* testing; F: Segment axial torsion under pure moment for FE model. FE results *versus* results of experimental studies, *in vitro* testing

FE 模型验证是 FE 建模过程中最重要的一步，Yoganandan 等[16]认为在负载-移位曲线基础上结合局部结构(如椎间盘)的动力学反应测试是 FE 模型验证最有效的方法。本研究 L_4～L_5 节段 FE 模型的轴向压缩-位移曲线、屈曲-旋转角度曲线、伸直-旋转角度曲线、侧屈-旋转角度曲线、扭曲-旋转角度曲线以及轴向压缩-椎间盘内压力曲线均处于相应实验生物力学研究结果范围或近似范围之内，证明所采用的基于 CAD 技术的腰椎表面模型建模方法、FE 模型各组分选用的单元类型和材料特性以及建模过程所做的各种特定假设均合理有效。经过充分验证的正常腰椎 L_4～L_5 节段有限元模型将成为个体化退变腰椎有限元模型库构建的平台和基础。

[参 考 文 献]

[1] Goel VK, Kim YE, Lim TH, et al. An analytical investigation of the mechanics of spinal instrumentation [J]. Spine, 1988, 13:1003-1111.

[2] Tatarajan RN, Andersson GB. The influence of lumbar disc height and cross-sectional area on the mechanical response of the disc to physiologic loading[J]. Spine, 1999, 24: 1873-1881.

[3] Teo EC, Lee KK, Ng HW, et al. Determination of load trans-

mission and contact force at facet joints of L_2-L_3 segment using FE method [J]. J Musculoskeletal Res, 2003, 7:97-109.

[4] Shirazi-Adl SA, Ahmed AM, Shrivastava SC. A finite element study of a lumbar motion segment subjected to pure sagittal plane moments [J]. J Biomech, 1986,19:331-350.

[5] Panjabi MM, Greenstein G, Duranceau J, et al. Three-dimensional quantitative morphology of lumbar spinal ligament [J]. J Spinal Disord, 1991,4:54-62.

[6] Brown T, Hansen RJ, Yorra AJ. Some mechanical tests on the lumbosacral spine with particular reference to intervertebral discs [J]. J Bone Joint Surg Am, 1957, 39-A(5):1135-1164.

[7] Markolf KL. Deformation of the thoracolumbar intervertebral joints in response to external load: a biomechanical study using autopsy material [J]. J Bone Joint Surg Am, 1972, 54: 511-533.

[8] Markolf KL, Morris JM. The structural components of the intervertebral disc. A study of their contributions to the ability of the disc to withstand compressive forces [J]. J Bone Joint Surg Am, 1974, 56: 675-687.

[9] Virgin WJ. Experimental investigations into the physical properties of the intervertebral disc [J]. J Bone Joint Surg Br, 1951, 33-B(4): 607-611.

[10] Nachemson A. Lumbar intradiscal pressure, experimental studies on post-mortem material [J]. Acta Orthop Scand, 1960, Suppl 43: 1-104.

[11] Rolander SD. Motion of the lumbar spine with special reference to the stabilizing effect of posterior fusion. An experimental study on autopsy specimens [J]. Acta Orthop Scand, 1966, Suppl 90: 1-144.

[12] Tencer AF, Ahmed AM, Burke DL. Some static mechanical properties of the lumbar intervertebral joint: intact and injured [J]. Biomech Eng, 1982,104: 193-201.

[13] White AA, Krag M, Panjabi MM, et al. Effect of preload on load displacement curves of the lumbar spine [J]. Orthop Clin North AM,1977, 8:181-192.

[14] Schultz AB, Warwich DN, Berkson MH, et al. Mechanical properties of human lumbar spine motion segments part 1: responses in flexion, extension, lateral bending, and torsion [J]. J Biomech Eng, 1979, 101:46-52.

[15] Andersson GB, Schultz AB. Effects of fluid injection on mechanical properties of intervertebral discs [J]. J Biomech, 1979,12:453-458.

[16] Yoganandan N, Kumaresan S, Voo L. Finite element applications in human cervical spine modeling [J]. Spine, 1996,21: 1824-1834.

[收稿日期] 2005-11-05 **[修回日期]** 2006-04-29

[本文编辑] 孙 岩

Clinical and prognostic analysis of ossified ligamentum flavum in a Chinese population

He S, Hussain N, Li S, Hou T (Department of Orthopedic Surgery, Changhai Hospital, Second Military Medical University, Shanghai 200433, China)

[**ABSTRACT**] Object: The authors performed a retrospective study of clinical and radiological data obtained in 27 Chinese patients with myelopathy induced by ossification of the ligamentum flavum (OLF) who underwent surgery between March 1990 and March 2002. The factors related to surgical outcome of thoracic OLF-induced myelopathy were also assessed. Methods: The preoperative clinical features and radiological findings were reviewed retrospectively. Preoperative and postoperative neurological status was assessed using the Japanese Orthopaedic Association (JOA) scoring system and the Nurick Scale. The ossified lesions were classified into five types (lateral, extended, enlarged, fused, and tuberous). Multiple linear regression and logistic regression analyses were performed to establish the factors affecting surgical outcome. The patients' chief complaints were lower-limb weakness and gait disturbance (93%), numbness and sensory deficit (89%), and low-back pain (48%). The coexisting pathological entities were disc herniation, canal stenosis, and ossification of posterior longitudinal ligament. The ossified ligamentum flavum was mainly located at the T10-12 (67%) and T1-3 (15%) levels. Symptoms in 26 patients improved but resolved completely in only 14 after surgery. The mean overall JOA score was 5.3±1.9 preoperatively and 7.9±2.3 postoperatively. There is a significant difference between the pre- and postoperative neurological status ($P<0.05$) determined by the Student t-test. The recovery rate was (46.3±9.4)%. Multiple regression analysis revealed negative correlation between the duration of preoperative symptoms and surgical outcome as well as a positive correlation between the preoperative JOA score and surgical outcome. Logistic regression analysis demonstrated that fecal and/or urinary incontinence, positive patellar and/or ankle clonus, and intramedullary high T2-weighted magnetic resonance (MR) imaging signal change had negative effects on the surgical outcome. Conclusions: The clinical and radiological features of OLF in the Chinese population are similar to those observed in the Japanese population. The duration of preoperative symptoms and JOA score are the most important predictors of the postoperative JOA score and recovery rate. The patients with fecal and/or urinary incontinence, positive patellar and/or ankle clonus, and intramedullary high T2-weighted MR imaging signal change were at higher risk of poor outcome after surgery.

[J Neurosurg Spine, 2005, 3: 348-354]